Spin-dependent shot noise in MgO-based magnetic tunnel junctions under noncollinear magnetization alignment

Yiou Zhang and Gang Xiao[*]

Department of Physics, Brown University, Providence, Rhode Island 02912, USA

We report experimental measurements of shot noise in MgO-based magnetic tunnel junctions (MTJs) upon angular magnetization rotation in the free layer. The normalized shot noise (the Fano factor) is found to be sub-Poissonian and exhibits a sinusoidal-like variation over the relative magnetic orientation between the free and the pinned layer inside the MTJs. The observed sub-Poissonian statistics provides direct evidence of electron sequential tunneling mediated by localized states inside the tunnel barrier. The variation of the Fano factor can be interpreted in terms of a semi-classical model that we propose. Based on this model, the variation of the Fano factor can be used to reveal microscopic details of the tunneling barrier.

I. INTRODUCTION

Over the last decade, measurements of electronic fluctuations or noise have been shown to be useful for investigating quantum transport in micro- and nano-scale structures. For example, shot-noise measurements were carried out to measure the transport of fractional charges in the quantum Hall systems of two-dimensional electron gases [1,2] and to study the transport of Cooper pairs in superconductor-normal metal junctions [3]. In spintronics, the study of noise can also be insightful and has received much attention [4–12]. For example, the intrinsic noise of magnetic tunnel junctions (MTJs) determines the magnetic-field sensing capability of MTJ-based sensors [13,14]. The study of noise can also provide more information on microscopic mechanisms than simple transport measurements. Specifically, shot noise allows for the direct measurement of the correlation in a current of discrete charges in MTJs [4–12]. In the case of totally uncorrelated electronic current, one observes the full or Poissonian shot noise with a power spectral density given by $2qIR^2$, where q is the electron charge, I is the average current, and R is the junction resistance. A relevant physical quantity, the normalized shot noise, or the Fano factor, is defined as $F = S_v/2qIR^2$, where S_v is the measured noise density. Using the Landauer-Buttiker formalism [15], it can be shown that, if an additional source of negative correlation is introduced, the shot noise amplitude should be reduced, i.e., $F \leqslant 1$.

Although the Fano factor in MTJs has been studied before, there is much controversy over its nature and discrepancy in its value. Jiang *et al.* [8] reported the observation of full shot noise ($F \approx 1$) in MTJs (CoFe/AlO$_x$/NiFeCo) with the anti-parallel magnetic alignment of ferromagnetic electrodes. Later, the same group measured a strong suppression of shot noise ($F \approx 0.45$) in MTJs with the same structure [9]. Guerrero *et al.* [5] reported Fano factors $F \approx 1$ and $F \approx 0.65$ in amorphous Al$_2$O$_3$-based tunnel junctions (Co/AlO$_x$/Py), without and with Cr-doping, respectively. From these results,

they suggested that the suppression of Fano factor arises from electrons passing through impurity states inside the tunnel barrier. In contrast, Garzon *et al.* [10] measured an enhanced Fano factor in tunnel junctions (Co/AlO$_x$/Co), which are believed to be due to a strong Coulomb interaction between tunneling electrons within the barrier. Sekiguchi *et al.* showed that MgO-based junctions (CoFeB/MgO/CoFeB) with epitaxial interfaces exhibit full shot noise [11].

In this paper, we study the variation of shot noise as we change the angle between the magnetization vectors of the free and the pinned electrodes in MgO-based MTJs. We have observed a sinusoidal-like variation of the Fano factor as a function of the angular magnetic configurations. In contrast with a linear model predicted by Tserkovnyak *et al.* [12], the observed Fano factor variation is consistent with our spin-dependent transport model. In this model, we conjectured that electronic transport occurs via an island inside the tunnel barrier in the spin-blockade regime [16–21]. Based on our model, the multimodal variation of the Fano factor can be a useful tool to understand the microscopic details of MTJs.

II. EXPERIMENT

We deposited MTJ multilayer films on thermally oxidized silicon wafers using a custom multi-target high-vacuum magnetron sputtering system with a base pressure of 2×10^{-8} Torr. The MTJ stack has the following structure (thicknesses in angstroms): Si/SiO$_2$/Ta(50)/Ru(300)/Ta(50)/ CoFe(20)/IrMn(150)/CoFe(20)/Ru(8)/CoFeB(30)/MgO(23)/ CoFeB(30)/Ta(50)/Ru(100). All layers except the MgO barrier were deposited by using DC sputtering at a constant Ar pressure of 2.05 mTorr. The MgO barrier was deposited by rf magnetron sputtering at an Ar pressure of 1.1 mTorr. During the sputtering process, we rotated the substrates at a constant speed to improve thickness uniformity over each wafer. Micron-size elliptical junctions with lateral dimensions of 2×4 μm^2 were patterned by using standard photolithography and a physical ion-beam milling process. Finally, we annealed the MTJs at 310 °C for 4 hours in a vacuum of 8×10^{-8} Torr
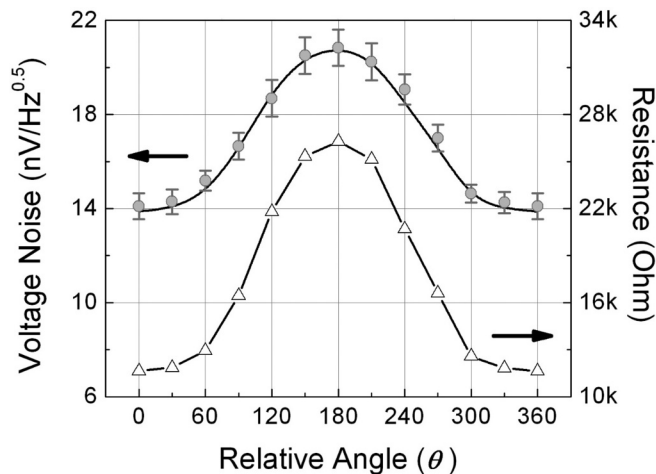
_____

*Gang_Xiao@Brown.edu

FIG. 1. Resistance (labeled by triangles) and Johnson-Nyquist noise (labeled by solid circles) of a MTJ as a function of the relative angle between the magnetization vectors of the ferromagnetic electrodes. Theoretical predictions for the resistance and Johnson noise are also plotted as solid lines. The error bar represents the experimental error from 10 power spectra taken for each angle.

under an applied in-plane magnetic field of 4.5 kOe, to improve the crystalline structures and to establish the magnetic pinning axis of the bottom magnetic electrode.

The noise measurements were carried out in an electro-magnetically shielded box. We used batteries to power the MTJs to minimize power-line noise in the setup and employed a two-channel time cross-correlation method to measure the noise spectrum from the MTJs. The signal from each channel was boosted by an amplifier with an intrinsic noise of $1.3 \, \mathrm{nV/Hz^{1/2}}$ at 1 Hz, and fed into a two-channel dynamic spectral analyzer (HP 35670A). The MTJ samples were subjected to a two-dimensional rotating magnetic field provided by a pair of permanent magnets mounted on a rotational platform. The strength of the rotating field at 100 Oe causes the magnetic moment of the free electrode to rotate with the rotating field direction, but it does not disturb the magnetic

moment of the pinned electrode. Using the method, we can control the angle between the two magnetic magnetization vectors.

III. RESULTS

We measured the resistance of the MTJ samples as a function of the relative angle between the magnetization vectors of ferromagnetic electrodes as shown in Fig. 1. According to magneto-tunneling theory [22], the electrical conductance G can be expressed as a linear function of the cosine of the angle θ between the magnetic moments of the free and pinned layers: $G = G_0(1 + p^2 \cos\theta)$, where G_0 is a constant, and p is the spin polarization of tunneling electrons. The resistance of the MTJ is its inverse. In Fig. 1, a solid line representing the theoretical value is plotted against the experimental data. The close match between theoretical and experimental value indicates that the pinned layer is not disturbed, while the free layer is fully aligned with the external magnetic field. Our early work [13] on MTJs with similar structures also shows a saturation field less than 100 Oe. This justifies our assumption that the free layer is fully aligned by the rotating magnets. In addition, we measured the Johnson-Nyquist noise by disconnecting the bias voltage from the MTJ samples. The power spectral density for Johnson noise is $S_v = 4k_B T R$, where k_B is Boltzmann's constant, R is the junction resistance, and T is the temperature. In Fig. 1, we show the experimental and theoretical values for the Johnson noise. The error bar represents the experimental error from 10 power spectra taken for each angle.

Upon applying a bias voltage to the MTJ sample, it begins to produce noise that arises from field-assisted barrier crossing rather than thermally assisted barrier crossing. Based on the semi-classical statistical mechanics approach [23], the noise spectrum can be described by the following equation:

$$S_v = 2qVR \coth\left(\frac{qV}{2k_B T}\right) + \frac{\alpha V^2}{A f^\gamma}, \qquad (1)$$

where the first term represents the thermal and shot noise, and the second term represents the $1/f$ noise. In Eq. (1),
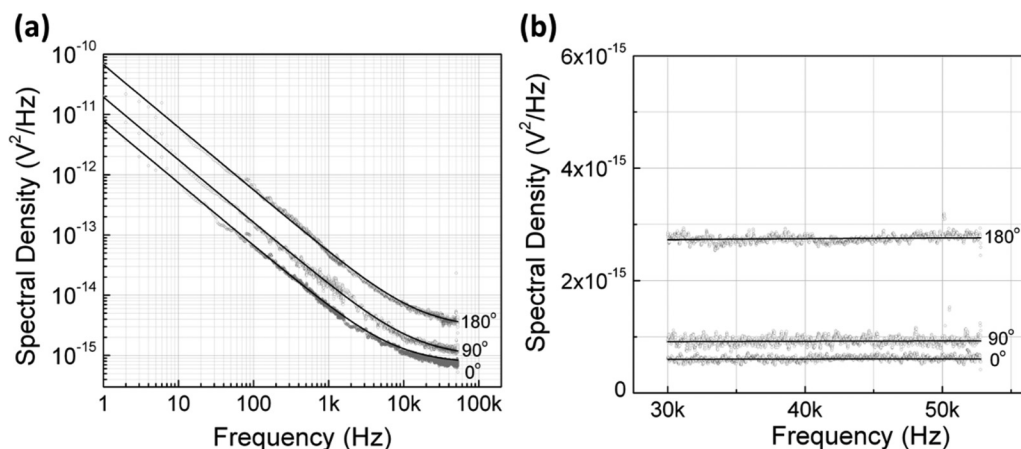

FIG. 2. (a) Noise power spectral density for a MTJ sample with the relative orientation between the magnetic moments at 0°, 90°, and 180°. The measurements were performed at constant current $I = 20 \, \mu$A (bias voltages were 0.232, 0.328, and 0.531 V, respectively), set by a resistor in series with MTJ. The open circles denote the experimental data, and the solid lines denote the mathematical fit. (b) The spectrum shows the frequency-independent component of the device noise. The $1/f$ noise is subtracted away according to Eq. (1).

V is the bias voltage, q is the electron charge, and k_B is Boltzmann's constant. When $qV \ll k_B T$, the MTJ produces only thermal Johnson noise. When the $\coth(qV/2k_B T)$ term approaches unity at higher voltages ($V > 150$ mV), shot noise becomes dominant [24]. In the second term, A is the area of the junction, f is the frequency, γ is the exponent (usually around 1), and α is a Hooge-like parameter [19]. In the low-frequency range, the $1/f$ noise component is dominant in the power spectral density (PSD). Figure 2 shows the PSDs for an MTJ sample with three different magnetic configurations. In Fig. 2(a), the $1/f$ noise is prominent, with the power spectral density inversely proportional to the frequency. Figure 2(b) shows the frequency-independent component of the device noise. The uncertainty in evaluating the frequency-independent part is determined by the noise spectral fluctuations amid the fitting lines. In our case, it is about 4.2×10^{-17} V^2/Hz.

After subtracting the $1/f$ noise from the noise spectrum, we obtain the shot noise as a function of the relative angle θ between the magnetization vectors of ferromagnetic electrodes. We present this result in Fig. 3(a). Each point depicts the Fano factor at the particular angle, with the error bar representing its standard deviation. The solid line shows the fitted Fano factor using a theoretical model, which will be discussed later. An interesting observation is that the Fano factor is smaller in the anti-parallel (AP) configuration than that in the parallel (P) configuration and that the valleys of the Fano factor curve are positioned at $\theta = 120°$ and $240°$. A quantitative explanation for the shape and multimodal variation of the Fano factor curve will be provided in the next section. In Fig. 3(b), we present the Fano factor measurements on two other similar MTJ samples, and the relative angle are fixed at 0, 90°, 180°, 270°, 360°. While each sample shows quantitative difference, these three curves are qualitatively similar. The multimodal Fano factor pattern presented here is intrinsic to the electron transport of MTJs and cannot be explained away by a particular deposition or patterning process of each individual MTJ sample.

IV. DISCUSSION

To explain the spin-dependent shot noise in MTJ systems, we assume that the electron transport for a MTJ sample depends on a collection of single-electron tunneling events, each of which is characterized by a Poissonian probability distribution. For an electron passing from the left reservoir (L) to the right reservoir (R) through a tunnel barrier (B), the average current is given by

$$I = \frac{e}{\langle t \rangle}, \quad (2)$$

and the Fano factor can be obtained by using a semi-classical theory for sequential tunneling [10,25],

$$F = \frac{\langle t^2 \rangle}{\langle t \rangle^2} - 1, \quad (3)$$

where the expectation value $\langle f(t) \rangle$ is defined as $\int_0^\infty f(t)P(t)dt$, and $P(t)$ is the probability density that two successive tunneling processes ($L \rightarrow B \rightarrow R$) occur at a time interval t.
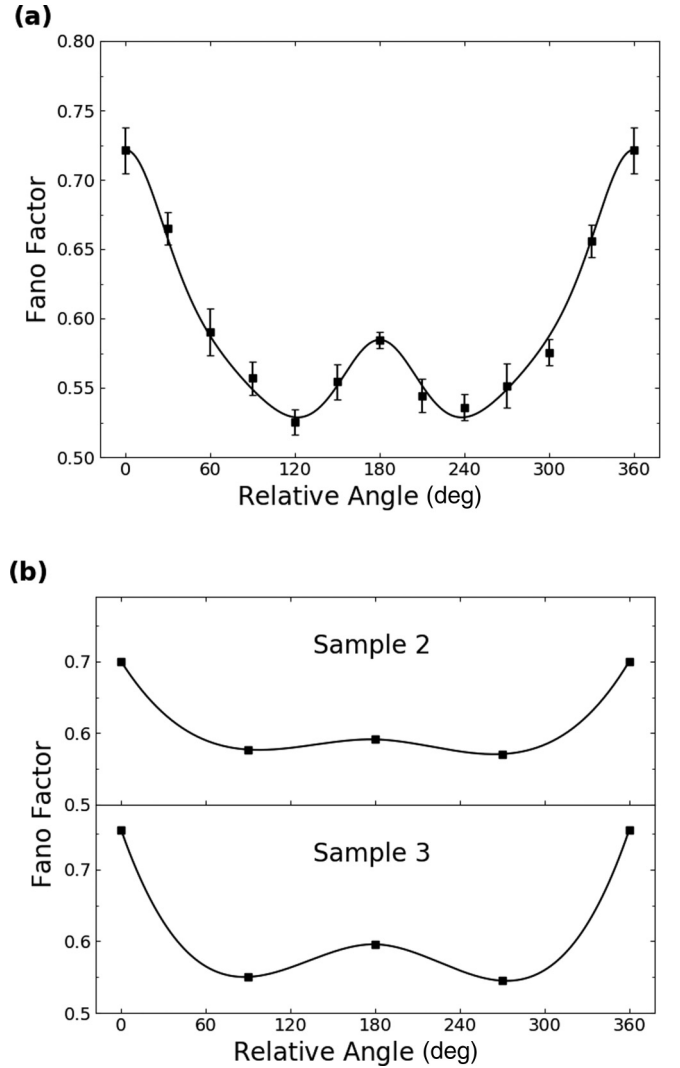

(a)

(b)

FIG. 3. (a) Fano factor as a function of the relative angle between the magnetization vectors of the ferromagnetic electrodes. The error bars represent the standard deviation. A theoretical fitting curve is also plotted for comparison, which is discussed in the text. (b) Fano factor measurements performed on two other similar MTJ samples. The solid lines connecting the squares are to guide the eye.

If the tunnel barrier has one localized state A, we can define the tunneling rate Γ_{iL} for hopping from L to A, and Γ_{iR} for hopping from A to R (i corresponds to spin $\uparrow$ and spin $\downarrow$, respectively). We further assume that once an electron with a particular spin hops into the localized state, then the state will become unavailable for electrons with the other spin [10]. In other words, minority-spin electrons with lower tunneling rates may block the transport of majority spins with higher tunneling rates. Including this "spin blockade" effect [16,17], the probability density can be expressed as

$$P(t) = \int_0^t dt' e^{-\Gamma_{\uparrow L} t'} e^{-\Gamma_{\downarrow L} t'}$$
$$\times (e^{-\Gamma_{\uparrow R}(t-t')} \Gamma_{\uparrow L} \Gamma_{\uparrow R} + e^{-\Gamma_{\downarrow R}(t-t')} \Gamma_{\downarrow L} \Gamma_{\downarrow R}). \quad (4)$$

Following the work of Garzon et al. [10], we define coefficients α, β, and γ such that $\Gamma_{\uparrow L} = \alpha \Gamma_{\uparrow R} = \beta \gamma \Gamma_{\downarrow L} = \beta \alpha \Gamma_{\downarrow R}$,

which gives the Fano factor as

$$F = \frac{2\beta^2\gamma + \beta\left[\frac{\gamma^2}{\alpha^2} + (1-\gamma)^2\right] + 2\gamma}{\beta\left(1 + \frac{\gamma}{\alpha} + \gamma\right)^2}. \tag{5}$$

Parameters α and α/γ describe the ratios of the left tunneling rate to the right tunneling rate for spin $\uparrow$ and spin $\downarrow$ electrons, while β describes the ratio of the right tunneling rate for spin $\uparrow$ electrons to that for spin $\downarrow$ electrons.

Now let us consider a large exchange-energy splitting along a certain direction Θ in the localized state A, where only spins polarized along Θ are energetically allowed to tunnel through [5]. In the simplest case, the left and right reservoirs are the pinned layer and free layer of an MTJ, respectively, and Θ is aligned with the magnetization of the pinned layer (say, spin $\uparrow$) due to the thermal magnetic annealing. When annealed at a high temperature, the spins of each individual atom in the localized structure will align with the externally applied field. This spin-field interaction will begin to reorganize the atoms somewhat, due to the spin-orbit interaction before it reaches equilibrium within this field. When the temperature is reduced, then, the atoms become "locked or frozen" once again, and the structure attains a new magnetization direction,

which is parallel to that of the pinned layer. Therefore, we can write the left tunneling rates as $\Gamma_{\uparrow L} = \gamma_L(1 + p)$ and $\Gamma_{\downarrow L} = \gamma_L(1 - p)$, where p is the spin polarization and γ_L is the average tunneling rate for an electron hop ($L \to A$). For the right tunneling rates, they are dependent on the relative angle θ of the magnetization vector of the right reservoir [26], i.e., $\Gamma_{\uparrow R} = \gamma_R(1 + p\cos\theta)$ and $\Gamma_{\downarrow R} = \gamma_R(1 - p\cos\theta)$, where p is the same for both reservoirs, and γ_R has a similar definition as γ_L. Note that $\theta = 0$ corresponds to the *P* state, and $\theta = 180°$ corresponds to the *AP* state.

Now,

$$\alpha = \frac{\Gamma_{\uparrow L}}{\Gamma_{\uparrow R}} = \frac{\gamma_L}{\gamma_R}\frac{1+p}{1+p\cos\theta},$$

$$\frac{\alpha}{\gamma} = \frac{\Gamma_{\downarrow L}}{\Gamma_{\downarrow R}} = \frac{\gamma_L}{\gamma_R}\frac{1-p}{1-p\cos\theta},$$

$$\beta = \frac{\Gamma_{\uparrow R}}{\Gamma_{\downarrow R}} = \frac{1+p\cos\theta}{1-p\cos\theta},$$

$$\gamma = \frac{1+p}{1-p}\frac{1-p\cos\theta}{1+p\cos\theta}.$$

Plugging these parameters into the expression for the Fano factor in Eq. (5), we have

$$F = \frac{4\gamma_L^2 + \gamma_R^2 - 8\gamma_L^2 p^2\cos\theta - 2p^2\left[2\gamma_L^2(p^2-2) + \gamma_R^2\right]\cos^2\theta + p^4\gamma_R^2\cos^4\theta}{(2\gamma_L + \gamma_R - 2\gamma_L p^2\cos\theta - p^2\gamma_R\cos^2\theta)^2}. \tag{6}$$

When $p = 0$, Eq. (6) reduces to the case of nonmagnetic tunnel barriers. When $p \neq 0$ and $\theta = 0$, Eq. (6) gives F_P for the P state [16] and, for $\theta = 180°$, it gives F_{AP} for the AP state [10]. By fixing the spin polarization, we can plot in

Fig. 4 the Fano factor as a function of θ and the ratio of the tunneling rate on a logarithmic scale, ($\log_{10}\gamma_R/\gamma_L$). When spin polarization is small, for example, $p = 0.2$ in Fig. 4(a),
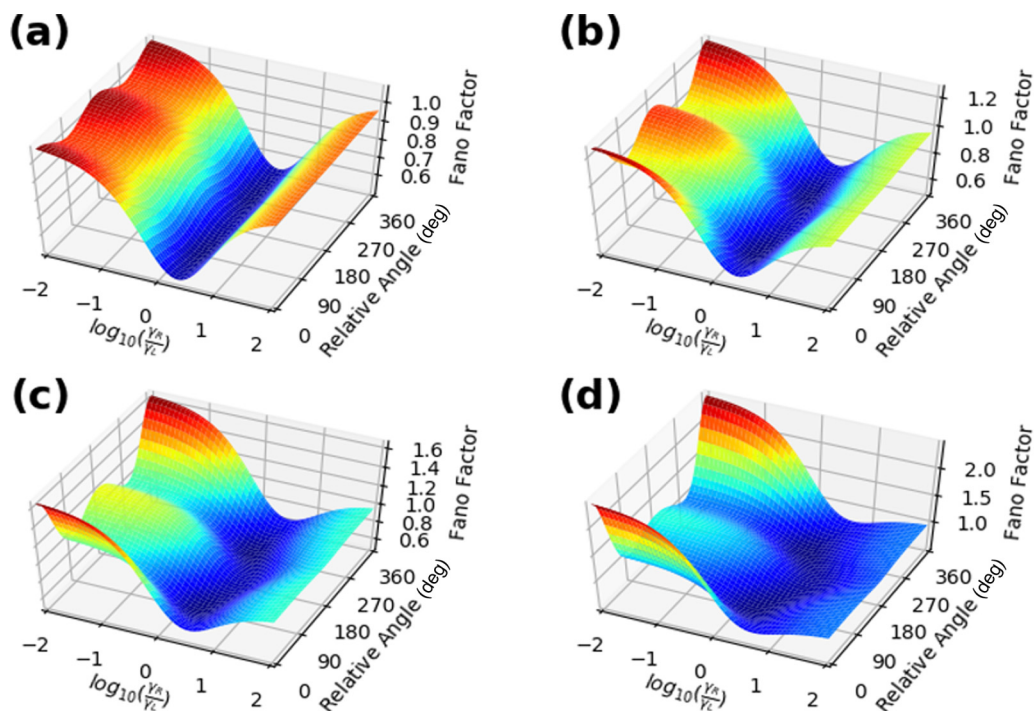

FIG. 4. Fano factor as a function of the ratio between the tunneling rates on a logarithmic scale, $\log_{10}(\gamma_R/\gamma_L)$, and the relative orientation between the magnetic moments of ferromagnetic electrodes θ, for the spin polarization $p = 0.2$ (a), 0.35 (b), 0.5 (c), and 0.65 (d).

variation of the Fano factor with θ is less significant. This indicates that the sinusoidal-like variation is indeed related to spin-dependent tunneling. As spin polarization gets larger, complex patterns and enhanced Fano factors appear at low $\log_{10}\gamma_R/\gamma_L$ where the spin-blockade effect is more prominent. Also, F_{AP} is less than F_P under such a condition, consistent with our measurement. Fitting of the experimental data in Fig. 3(a) gives $\log_{10}\gamma_R/\gamma_L = 0.58$ and $p = 0.6498$. Note that the tunneling magnetoresistance ratio (TMR) of this sample is 125%, from which we obtain a spin polarization of $p = 62\%$ according to $TMR = 2p^2/(1 - p^2)$. This value is consistent with the p parameter obtained from the fitting in Fig. 3(a).

Since the tunneling rate depends exponentially on the barrier thickness, the ratio of the tunneling rate in the logarithmic scale corresponds to a linear scale for the position of the localized state inside the tunnel barrier. A small ratio corresponds to the proximity to the left reservoir **L** and large ratio to the right reservoir **R**. As a result we can use the Fano factor pattern to reveal the microscopic details of the tunnel barrier of a MTJ device**.** To see this quantitatively, we calculate Fano factor versus θ for different values of $\log_{10}\gamma_R/\gamma_L$ and p. Besides the valley position of the Fano factor curve, the "depth" of the valley is also important. We characterize the valley depth by the relative difference between the Fano factor minimum (F_{min}) and the Fano factor at the **AP** state (F_{AP}): $(F_{AP} - F_{min})/F_{min}$. The valley position and depth are plotted in Fig. 5. As shown in Fig. 5(a), the valley position varies between $80°$ and $180°$. Interestingly, the valley position depends strongly on $\log_{10}\gamma_R/\gamma_L$, yet only slightly on p. When $\gamma_R \gg \gamma_L$, the localized state is close to the right reservoir **R**, and **L** $\to$ **A** tunneling is negligible. Since sequential tunneling is minimal, full shot noise ($F \approx 1$) is expected regardless of spin polarization. On the other hand, if $\gamma_R \ll \gamma_L$, the spin-blockade effect is dominant [18–21], which gives rise to the sinusoidal-like variation of the Fano factor. While valley position depends mostly on the ratio of the tunneling rates and thus the position of the localized state inside the tunneling barrier, valley depth shows strong dependence on spin polarization. The valley depth gets larger at larger spin polarization, except for $\gamma_R \ll \gamma_L$. By measuring the Fano factor as a function of relative orientation of magnetization of the two ferromagnetic electrodes, we can reveal the microscopic details of MTJs, which are difficult to know from simple transport measurements.

V. CONCLUSIONS

We have measured the shot noise in MgO-based MTJs with a continuous change in the relative magnetization alignments of the two ferromagnetic layers (free and pinned). The normalized shot noise (Fano factor) is suppressed and exhibits a strong dependence on the relative orientation between the magnetization vectors of ferromagnetic electrodes. The observations can be quantitatively explained by considering a probabilistic model of sequential tunneling, in which electrons pass through a localized state inside the tunnel barrier with spin-dependent tunneling rates. The anti-correlation in the current, which by itself is due to the finite dwell time for an electron staying at the localized state and the spin-blockade effect, reduces the shot-noise amplitude and causes a
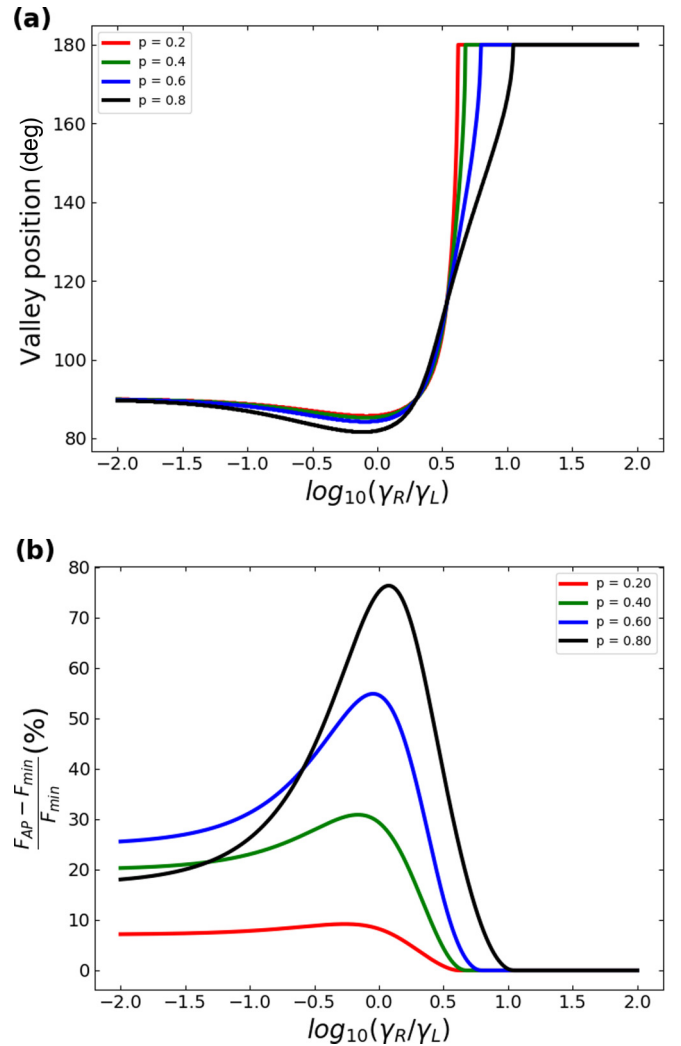

FIG. 5. (a) Valley position and (b) valley depth in the Fano factor curve as a function of the ratio of tunneling rates on a logarithmic scale, $\log_{10}(\gamma_R/\gamma_L)$, for various spin polarizations p.

sinusoidal-like variation of the Fano factor. Through measurement of the Fano factor at different magnetization alignments, the microscopic details of the tunneling barrier can be revealed. Such information would be hard, if not impossible, to obtain from simple transport measurements or other characterization techniques. Besides shot noise, the low-frequency $1/f$ noise of the MTJ also shows strong dependence on the quality of the tunnel barrier [27,28]. Therefore, characterizing barrier quality through shot noise measurement would also be beneficial to the low-frequency application of MTJ-based sensor. We believe our results could provide important insight into the magneto-tunneling process in MTJs and a guideline for improving the performance of MTJ-based devices.

[1] R. de Picciotto, M. Reznikov, M. Heiblum, V. Umansky, G. Bunin, and D. Mahalu, Nature (London) **389**, 162 (1997).

[2] L. Saminadayar, D. C. Glattli, Y. Jin, and B. Etienne, Phys. Rev. Lett. **79**, 2526 (1997).

[3] X. Jehl, M. Sanquer, R. Calemczuk, and D. Mailly, Nature (London), **405**, 50 (2000).

[4] P. K. George, Y. Wu, R. M. White, E. Murdock, and M. Tondra, Appl. Phys. Lett. **80**, 682 (2002).

[5] R. Guerrero, F. G. Aliev, Y. Tserkovnyak, T. S. Santos, and J. S. Moodera, Phys. Rev. Lett. **97**, 266602 (2006).

[6] A. L. Chudnovskiy, J. Swiebodzinski, and A. Kamenev, Phys. Rev. Lett. **101**, 066601 (2008).

[7] R. Guerrero, D. Herranz, F. G. Aliev, F. Greullet, C. Tiusan, M. Hehn, and F. Montaigne, Appl. Phys. Lett. **91**, 132504 (2007).

[8] L. Jiang, E. R. Nowak, P. E. Scott, J. Johnson, J. M. Slaughter, J. J. Sun, and R. W. Dave, Phys. Rev. B **69**, 054407 (2004b).

[9] L. Jiang, J. F. Skovholt, E. R. Nowak, and J. M. Slaughter, Proc. SPIE **5469**, 13 (2004).

[10] S. Garzon, Y. Chen, and R. A. Webb, Physica E **40**, 133 (2007).

[11] K. Sekiguchi, T. Arakawa, Y. Yamauchi, K. Chida, M. Yamada, H. Takahashi, D. Chiba, K. Kobayashi, and T. Ono, App. Phys. Lett **96**, 252504 (2010).

[12] Y. Tserkovnyak and A. Brataas, Phys. Rev. B **64**, 214402 (2001).

[13] W. Z. Zhang, Q. Hao, and G. Xiao, Phys. Rev. B **84**, 094446 (2011).

[14] Y. Zhang, G. He, X. Zhang, and G. Xiao, Appl. Phys. Lett. **115**, 022402 (2019).

[15] Y. M. Blanter and M. Buttiker, Phys. Rep. **336**, 1 (2000).

[16] M. Braun, J. Konig, and J. Martinek, Phys. Rev. B **74**, 075328 (2006).

[17] B. R. Bulka, Phys. Rev. B **62**, 1186 (2000).

[18] B. R. Bulka, J. Martinek, G. Michalek, and J. Barnas, Phys. Rev. B **60**, 12246 (1999).

[19] W. Belzig, Phys. Rev. B **71**, 161301(R) (2005).

[20] F. Elste and C. Timm, Phys. Rev. B **73**, 235305 (2006).

[21] A. Cottet, W. Belzig, and C. Bruder, Phys. Rev. Lett. **92**, 206801 (2004).

[22] J. C. Slonczewski, Phys. Rev. B **39**, 6995 (1989).

[23] D. Rogovin and D. J. Scalapino, Ann. Phys. **86**, 1 (1974).

[24] K. B. Klaassen, J. C. L. van Peppen, and X. Xing, J. Appl. Phys **93**, 8573 (2003).

[25] J. H. Davies, P. Hyldgaard, S. Hershfield, and J. W. Wilkins, Phys. Rev. B **46**, 9620 (1992).

[26] J. C. Slonczewski, Phys. Rev. B **71**, 024411 (2005).

[27] C. Ren, X. Y. Liu, B. D. Schrag, and G. Xiao, Phys. Rev. B **69**, 104405 (2004).

[28] G. Q. Yu, J. F. Feng, H. Kurt, H. F. Liu, X. F. Han, and J. M. D. Coey, J. Appl. Phys. **111**, 113906 (2012).